Coherent Quantum-Noise Cancellation for Optomechanical Sensors

Mankei Tsang* and Carlton M. Caves

Center for Quantum Information and Control, University of New Mexico, MSC074220, Albuquerque, New Mexico 87131-0001, USA

(Received 14 June 2010; published 13 September 2010)

Using a flow chart representation of quantum optomechanical dynamics, we design coherent quantum-noise-cancellation schemes that can eliminate the backaction noise induced by radiation pressure at all frequencies and thus overcome the standard quantum limit of force sensing. The proposed schemes can be regarded as novel examples of coherent feedforward quantum control.

DOI: 10.1103/PhysRevLett.105.123601 PACS numbers: 42.50.Wk, 03.65.Ta, 42.65.Yj

Noise introduces error to communication or sensing because it is unknown to the observer and cannot be distinguished from the desired signal. If the noise can be measured separately, one can physically or computationally remove the noise. This is the principle of noise cancellation, a technique that has seen widespread commercial application, especially for acoustic-noise control [1]; noise-cancelling headphones, for example, work by recording the ambient noise and playing it back with opposite amplitude to interfere destructively with the noise reaching the inner ear.

Here we consider the application of noise cancellation to quantum systems. We focus on optomechanical force sensors, in which quantum radiation-pressure fluctuations on a moving mirror within an optical cavity can introduce excess noise, called the backaction noise, in addition to the shot noise at the cavity output. This leads to the standard quantum limit on detecting a classical force on the mirror [2]. Various methods of quantum-noise reduction have been proposed to overcome the standard quantum limit, including frequency-dependent squeezing of the input light [3–7], variational measurement [5,7,8], introducing a Kerr medium inside the optical cavity [9], and the use of dual mechanical resonators [10,11] or an optical spring [12,13] to modify the mechanical response function. Several of these proposals have been implemented [6,11,13], though not in the quantum regime. All can be regarded as quantum-noise-cancellation (QNC) schemes, which utilize destructive interference to reduce or eliminate the effects of backaction. With backaction tamed, squeezing of the input light [14] can be used to improve sensitivity further.

To facilitate understanding of the QNC concept and design of new QNC schemes, we introduce the use of flow charts to depict the quantum dynamics. Using the flow charts, we design a few novel QNC schemes that can eliminate backaction noise at all frequencies and should require less space than previous broadband QNC schemes. Although the effects of quantum radiation-pressure noise are only now becoming detectable [15], the field of optomechanics has recently seen rapid progress [16]. Backaction noise is expected to become a major issue in future optomechanical sensors. Combined with quantum filtering and smoothing [17], QNC has the potential to improve significantly the performance of future force sensors beyond conventional quantum limits. In the context of quantum control [18], QNC schemes can be regarded as examples of *coherent feedforward* quantum control, to be contrasted with measurement-based feedforward control [19] and coherent feedback control [20] techniques.

Consider now a Fabry-Perot cavity with a moving mirror, as depicted in Fig. 1. The mirror is modeled optically as perfectly reflecting and mechanically as a harmonic oscillator with position operator $q(t)$, momentum operator $p(t)$, mass m, and resonant frequency ω_m, subject to a force $f(t)$. The cavity is pumped with an input beam $A_{\rm in}(t)$, incident on the partially transmitting mirror on the left. We work in a rotating frame that removes the harmonic time dependence at the input beam's carrier frequency ω_0. All phases are referenced to the input field, which has constant (real) mean amplitude $\langle A_{\rm in}\rangle = \mathcal{A}_{\rm in}$. The intracavity field decays at rate γ due to coupling through the partially transmitting mirror to the output beam $A_{\rm out}(t)$. The intracavity optical field $a(t)$ is assumed to be resonant at the carrier frequency ω_0 when the mirror is displaced to its equilibrium position under the mean radiation pressure, at which point the round-trip length is $2L$. The mirror position $q(t)$ is defined relative to this equilibrium position. The force is estimated by continuous homodyne measurement of an appropriate quadrature of $A_{\rm out}$, labeled 2 in the following and usually the phase quadrature. The operators obey canonical commutation relations: $[q(t), p(t)] = i\hbar$, $[a(t), a^\dagger(t)] = 1$, and $[A_{\rm in}(t), A_{\rm in}^\dagger(t')] = \delta(t - t')$.

One can generalize this basic setup to more elaborate configurations, e.g., more complicated optical and mechanical mode structures or detuned cavity excitation,

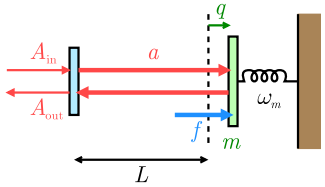

FIG. 1 (color online). Optomechanical force sensor.

which gives rise to an optical spring [12,13]. A major difference from a two-armed interferometer is that squeezed light must be input in the same beam as the mean field that powers the system. Nonetheless, this minimal setup already captures the salient features of cavity optomechanical systems.

The operator equations of motion are

$$\frac{dq}{dt} = \frac{p}{m}, \qquad \frac{dp}{dt} = -m\omega_m^2 q + \frac{\hbar\omega_0}{L}(a^\dagger a - \alpha^2) + f,$$
$$\frac{da}{dt} = -\gamma a + \frac{i\omega_0}{L} qa + \sqrt{2\gamma}A_{\rm in}, \qquad A_{\rm out} = \sqrt{2\gamma}a - A_{\rm in}, \tag{1}$$

where $\alpha = \mathcal{A}_{\rm in}\sqrt{2/\gamma}$ is the mean cavity field ($\langle a^\dagger a\rangle = \alpha^2$). Removing mean fields and defining amplitude and phase quadrature operators for the fluctuations that remain, $A_{\rm in} = \mathcal{A}_{\rm in} + (\xi_1 + i\xi_2)/\sqrt{2}$, $A_{\rm out} = \mathcal{A}_{\rm in} + (\eta_1 + i\eta_2)/\sqrt{2}$, and $a = \alpha + (a_1 + ia_2)/\sqrt{2}$, one can linearize Eqs. (1) by neglecting quadratic terms and obtain a system of linear differential equations:

$$\frac{d\boldsymbol{x}}{dt} = \boldsymbol{F}\boldsymbol{x} + \boldsymbol{G}\boldsymbol{w}, \qquad \boldsymbol{y} = \boldsymbol{H}\boldsymbol{x} + \boldsymbol{J}\boldsymbol{w}. \tag{2}$$

Here the *state variables* $\boldsymbol{x} \equiv (q \quad p \quad a_1 \quad a_2)^T$, inputs $\boldsymbol{w} \equiv (f \quad \xi_1 \quad \xi_2)^T$, and output signals $\boldsymbol{y} \equiv (\eta_1 \quad \eta_2)^T$ are related by the matrices

$$\boldsymbol{F} \equiv \begin{pmatrix} 0 & 1/m & 0 & 0 \\ -m\omega_m^2 & 0 & \hbar\kappa & 0 \\ 0 & 0 & -\gamma & 0 \\ \kappa & 0 & 0 & -\gamma \end{pmatrix},$$
$$\boldsymbol{J} \equiv \begin{pmatrix} 0 & -1 & 0 \\ 0 & 0 & -1 \end{pmatrix}, \qquad \boldsymbol{G} \equiv \begin{pmatrix} 0 & 0 & 0 \\ 1 & 0 & 0 \\ 0 & \sqrt{2\gamma} & 0 \\ 0 & 0 & \sqrt{2\gamma} \end{pmatrix}, \tag{3}$$
$$\boldsymbol{H} \equiv \begin{pmatrix} 0 & 0 & \sqrt{2\gamma} & 0 \\ 0 & 0 & 0 & \sqrt{2\gamma} \end{pmatrix},$$

where $\kappa \equiv \sqrt{2}\alpha\omega_0/L$ is an optomechanical coupling strength.

In control-system design, it is often illuminating to draw a block diagram to represent a system of differential equations [21]. Here we use a simpler depiction, which we call a flow chart, as shown in Fig. 2(a) for Eqs. (2) and (3). Arrows point from a variable on the right-hand side of an equation of motion to a connected variable on the left-hand side. Since the system is linear, the output signals are sums of independent contributions from the inputs, so one can easily depict the flow of signal and noise from input to output. In Fig. 2(a), the dashed arrows depict contributions to the output quadrature η_2 from the signal f and from the input amplitude and phase fluctuations ξ_1 and ξ_2. The ξ_2 contribution is commonly known as shot noise, while the ξ_1 contribution is the backaction noise due to the Kerr-like

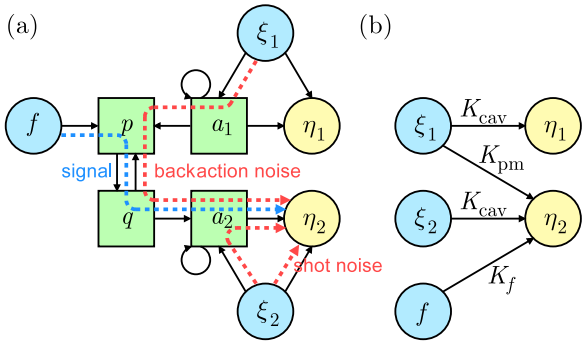

FIG. 2 (color online). (a) Flow chart representation of Eqs. (2) and (3). (b) Simplified flow chart depicting only the input and output signals linked by transfer functions.

ponderomotive coupling of the cavity amplitude quadrature a_1 to the phase quadrature a_2.

The solution for the state variables contains a transient solution, which decays exponentially and which can be ignored by pushing the initial time to $-\infty$. It is convenient to Fourier transform the remaining inhomogenous solution, by writing $\boldsymbol{y}(\Omega) = \boldsymbol{K}(\Omega)\boldsymbol{w}(\Omega)$, where the overall transfer matrix is

$$\boldsymbol{K}(\Omega) = -\boldsymbol{H}(i\Omega\boldsymbol{I} + \boldsymbol{F})^{-1}\boldsymbol{G} + \boldsymbol{J} = \begin{pmatrix} 0 & K_{\rm cav} & 0 \\ K_f & K_{\rm pm} & K_{\rm cav} \end{pmatrix}, \tag{4}$$

with $\boldsymbol{I}$ being the identity matrix. The cavity and ponderomotive transfer functions are

$$K_{\rm cav}(\Omega) = \frac{\gamma + i\Omega}{\gamma - i\Omega}, \qquad K_{\rm pm}(\Omega) = \frac{2\gamma\hbar\kappa^2/m}{(\omega_m^2 - \Omega^2)(\gamma - i\Omega)^2}, \tag{5}$$

respectively, and the signal transfer function is $K_f(\Omega) = K_{\rm pm}(\Omega)(\gamma - i\Omega)/\hbar\kappa\sqrt{2\gamma}$. A simplified flow chart that connects outputs to inputs by transfer functions is shown in Fig. 2(b).

Unruh's proposal for frequency-dependent input squeezing [3–7] and the Vyatchanin-Matsko variational-measurement scheme [5,7,8] can be understood by using flow charts. First consider Unruh's proposal, flow charted in Fig. 3(a). The input beam, with quadratures χ_1 and χ_2, is processed through a passive system that rotates the quadratures by a frequency-dependent angle $\phi(\Omega)$, after which the beam is displaced by $\mathcal{A}_{\rm in}$ to produce the input field $A_{\rm in}$ to the optical cavity. The transfer functions from χ_1 and χ_2 to the output phase quadrature η_2 are $K_{\eta_2\chi_1} = K_{\rm pm}\cos\phi + K_{\rm cav}\sin\phi$ and $K_{\eta_2\chi_2} = -K_{\rm pm}\sin\phi + K_{\rm cav}\cos\phi$. The rotation is chosen to make the contribution from χ_1 vanish, i.e., $K_{\eta_2\chi_1} = 0$, by introducing destructively interfering paths from χ_1 to η_2, as shown in Fig. 3(a). This requires $\tan\phi(\Omega) = -K_{\rm pm}(\Omega)/K_{\rm cav}(\Omega)$. Kimble *et al.* [5] devised a method for performing the dispersive rotation over a wide bandwidth by filtering the input beam through two detuned

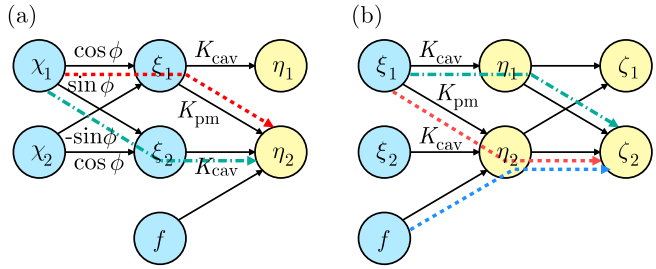

FIG. 3 (color online). (a) Frequency-dependent input squeezing. (b) Variational-measurement scheme.

cavities. If the input to the filtering cavities is vacuum, the rotation has no effect on sensitivity; since χ_2 is now entirely responsible for the output noise, however, it can be squeezed to improve the sensitivity to the shot-noise limit and beyond.

The variational-measurement scheme can be understood by using the flow chart in Fig. 3(b). This scheme dispersively rotates the output light and measures the final output quadrature ζ_2, which is a combination of the original output quadratures η_1 and η_2. This introduces an "antinoise" path from ξ_1 to ζ_2 via η_1, which can be used to cancel the original backaction noise path via η_2. Given the similarity of the flow charts in Fig. 3(a), the required dispersive rotation is the same as that for Unruh's proposal and can again be implemented by using two detuned cavities. With backaction noise eliminated, the sensitivity is limited by shot noise and can be improved further by squeezing the input quadrature ξ_2 [5].

While the aforementioned schemes can be regarded as examples of coherent QNC, it is clear from Fig. 2 that a more direct way of cancelling the backaction noise is to introduce an antinoise path from a_1 to a_2, as illustrated in Fig. 4. This calls for coherent processing of the intracavity field, by using parametric interactions to undo the ponderomotive squeezing. The use of a Kerr medium [9], the dual-mechanical-resonator scheme [10,11], and even an optical spring [12,13] can also be thought of as intracavity QNC schemes, but they cannot eliminate the backaction noise at all frequencies. To achieve broadband QNC, we introduce two *auxiliary* state variables q' and p', which play the role of q and p in the antinoise path, as shown in Fig. 4(c). Adjustable parameters g, μ, and ν, all with units of frequency, characterize the couplings in the antinoise path. The antinoise transfer function, indicated in Fig. 4(b) by the green dash-dotted arrow, is $2\gamma\mu g^2/(-\mu\nu-\Omega^2)\times(\gamma-i\Omega)^2=-K_{\rm pm}$. We need $\mu\nu=-\omega_m^2$ and $\mu g^2=-\hbar\kappa^2/m$, thus requiring μ to be negative. This cannot be implemented by ponderomotive coupling to another mechanical oscillator unless its mass is negative.

The matched squeezing can nonetheless be achieved by coupling the intracavity field to an auxiliary field $b\equiv(q'+ip')/\sqrt{2}$. The required parameters are $\nu=-\mu=\omega_m$ and $g=\kappa\sqrt{\hbar/m\omega_m}=\alpha\omega_0\sqrt{2\hbar/m\omega_m}/L$, and the

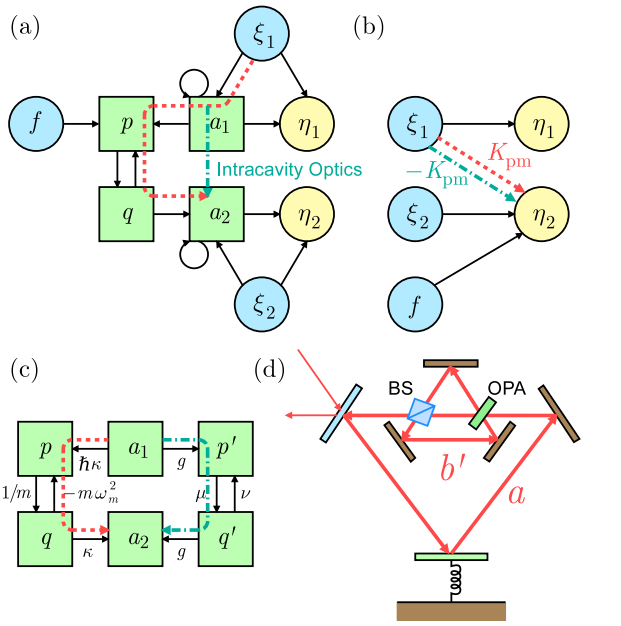

FIG. 4 (color online). (a) Backaction noise cancellation achieved by introducing an antinoise path (green dash-dotted arrow) from the intracavity amplitude quadrature a_1 to the phase quadrature a_2. (b) Simplified flow chart. (c) Detailed flow chart of the ponderomotive coupling and the intracavity matched squeezing. (d) An implementation of the matched squeezing scheme.

equations for a and b become

$$\frac{da}{dt}=-\gamma a+\frac{i\omega_0}{L}qa+\frac{ig}{2}(b+b^\dagger)+\sqrt{2\gamma}A_{\rm in},$$
$$\frac{db}{dt}=i\omega_m b+\frac{ig}{2}(a+a^\dagger)-ig\alpha. \tag{6}$$

The auxiliary field should be inside another optical cavity, with resonant frequency $\omega_0-\omega_m$; it plays the role of a *negative-energy* mode in the antinoise path. The constant driving term $-ig\alpha$, which removes the mean field from b, can be eliminated by redefining the auxiliary mode as $b'=b-g\alpha/\omega_m$ and displacing the input field $A_{\rm in}$, resulting in the following equations of motion:

$$\frac{da}{dt}=-\gamma a+\frac{i\omega_0}{L}qa+\frac{ig}{2}(b'+b'^\dagger)+\sqrt{2\gamma}A'_{\rm in},$$
$$\frac{db'}{dt}=i\omega_m b'+\frac{ig}{2}(a+a^\dagger),\qquad A'_{\rm in}=A_{\rm in}+i\mathcal{A}_{\rm in}\frac{g^2}{\gamma\omega_m}. \tag{7}$$

The coupling between a and b' can then be realized by using a beam splitter (BS) and an optical parametric amplifier (OPA), as schematically shown in Fig. 4(d). With the backaction noise removed, only the shot noise from ξ_2 remains, and one can improve sensitivity further by increasing the optical power or by squeezing ξ_2.

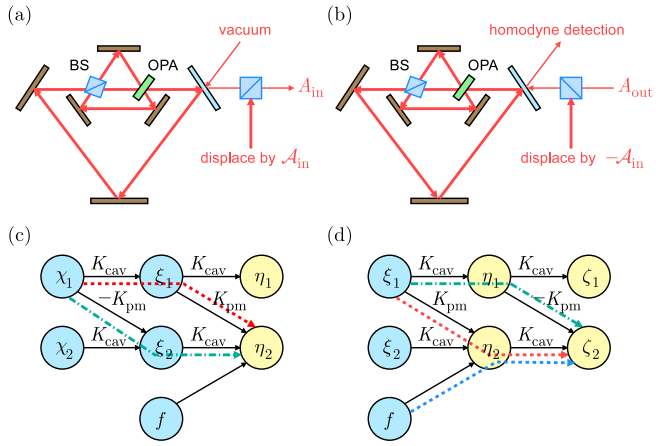

FIG. 5 (color online). Implementations of the (a) input and (b) output matched squeezing schemes and the associated flow charts (c) and (d). For a two-armed interferometer, one only needs to squeeze the dark input or output port and does not need to perform the displacement.

In terms of the coupling constant g, the ponderomotive transfer function has the form

$$K_{\rm pm}(\Omega) = \frac{g^2}{\gamma\omega_m}\frac{\omega_m^2}{\omega_m^2 - \Omega^2}\frac{2\gamma^2}{(\gamma - i\Omega)^2}, \qquad (8)$$

so $|K_{\rm pm}(\Omega)|/|K_{\rm cav}(\Omega)| \sim g^2/\gamma\omega_m$ for frequencies away from the mechanical resonance; backaction is thus important when $g \gtrsim \sqrt{\gamma\omega_m}$. The required single-pass idler gain of the OPA is thus $G \simeq (gL/c)^2 \gtrsim \gamma\omega_m(L/c)^2 \equiv G_0$. G_0 ranges from about $(2\pi \times 10\ \text{Hz} \times 5\ \text{km}/c)^2 \simeq 10^{-6}$ for gravitational-wave detectors to $(2\pi \times 50\ \text{MHz} \times 100\ \mu\text{m}/c)^2 \simeq 10^{-8}$ for microscale systems [16], so the required G should be easily achievable with current OPA technology.

There is another potential problem: The number of photons in the auxiliary cavity in Fig. 4(d) is $\langle b'^\dagger b'\rangle = g^2\alpha^2/\omega_m^2$, which becomes significantly higher than that in the primary cavity when ω_m is small, making the intracavity scheme problematic for applications that use high circulating power. This problem can be alleviated by using matched squeezing to modify the input or output optics. This requires the use of another double-cavity setup, similar to that in Fig. 4(d), but without the moving mirror, to presqueeze the input light going into the sensor cavity or postsqueeze the output light, as shown in Figs. 5(a) and 5(b). The flow charts for these schemes, shown in Figs. 5(c) and 5(d), demonstrate broadband cancellation of backaction noise much like the intracavity scheme. If one is interested only in low frequencies $\Omega \ll \gamma$, the input or output matched squeezing can be implemented by using smaller cavities with a larger decay rate γ and a larger coupling constant g, with g^2/γ held constant.

We have assumed an ideal system, neglecting intrinsic mechanical and optical losses, to illustrate the essential features of QNC. Such assumptions are unrealistic in practice. To assess QNC schemes, it will be important to take into account the fluctuations associated with dissipation, such as the thermal noise associated with mechanical damping. The design and performance of QNC in the presence of realistic dissipation and noise deserve further investigation.

We acknowledge discussions with T. Kippenberg and S. Waldman. This work was supported in part by NSF Grants No. PHY-0903953 and No. PHY-0653596 and ONR Grant No. N00014-07-1-0304.

*mankei@unm.edu

[1] C. H. Hansen, *Understanding Active Noise Cancellation* (Taylor & Francis, London, 2001).
[2] V. B. Braginsky and F. Ya. Khalili, *Quantum Measurement* (Cambridge University Press, Cambridge, England, 1992).
[3] W. G. Unruh, in *Quantum Optics, Experimental Gravitation, and Measurement Theory*, edited by P. Meystre and M. O. Scully (Plenum, New York, 1982), p. 647.
[4] R. S. Bondurant and J. H. Shapiro, Phys. Rev. D **30**, 2548 (1984); M. T. Jaekel and S. Reynaud, Europhys. Lett. **13**, 301 (1990); A. Luis and L. L. Sánchez-Soto, Phys. Rev. A **45**, 8228 (1992).
[5] H. J. Kimble *et al.*, Phys. Rev. D **65**, 022002 (2001).
[6] C. M. Mow-Lowry *et al.*, Phys. Rev. Lett. **92**, 161102 (2004).
[7] F. Ya. Khalili, Phys. Rev. D **81**, 122002 (2010), and references therein.
[8] S. P. Vyatchanin and A. B. Matsko, JETP **77**, 218 (1993); S. P. Vyatchanin and E. A. Zubova, Phys. Lett. A **201**, 269 (1995).
[9] R. S. Bondurant, Phys. Rev. A **34**, 3927 (1986).
[10] T. Briant *et al.*, Phys. Rev. D **67**, 102005 (2003).
[11] T. Caniard *et al.*, Phys. Rev. Lett. **99**, 110801 (2007).
[12] A. Buonanno and Y. Chen, Phys. Rev. D **64**, 042006 (2001); **65**, 042001 (2002).
[13] P. Verlot *et al.*, Phys. Rev. Lett. **104**, 133602 (2010).
[14] C. M. Caves, Phys. Rev. D **23**, 1693 (1981).
[15] P. Verlot *et al.*, Phys. Rev. Lett. **102**, 103601 (2009).
[16] T. J. Kippenberg and K. J. Vahala, Science **321**, 1172 (2008); F. Marquardt and S. M. Girvin, Physics **2**, 40 (2009).
[17] M. Tsang, Phys. Rev. Lett. **102**, 250403 (2009).
[18] H. Mabuchi and N. Khaneja, Int. J. Robust Nonlinear Control **15**, 647 (2005), and references therein.
[19] P. K. Lam *et al.*, Phys. Rev. Lett. **79**, 1471 (1997); U. L. Andersen and R. Filip, in *Progress in Optics*, edited by E. Wolf (Elsevier, Amsterdam, 2009), Vol. 53, p. 365, and references therein.
[20] M. R. James, H. I. Nurdin, and I. R. Petersen, IEEE Trans. Autom. Control **53**, 1787 (2008).
[21] G. F. Franklin, J. D. Powell, and A. Emami-Naeini, *Feedback Control of Dynamic Systems* (Prentice-Hall, Upper Saddle River, NJ, 2002).